Design and Analysis of an Active Airbrake System for Apogee Control in a 10,000-ft Class Suborbital Rocket

Yuvasurya R. Vangala* and Alonso Arregui Martinez†
Georgia Institute of Technology, Atlanta, Georgia, 30332

Achieving precise apogee targeting in high-power suborbital rockets is challenging due to uncertainties in motor performance, atmospheric conditions, and vehicle mass properties that are difficult to correct prior to launch. This paper presents the design and analysis of an active airbrake system developed to mitigate these uncertainties during flight and improve apogee accuracy for a 10,000-ft class rocket. The system employs symmetrically deploying aerodynamic plates that extend radially from the airframe to modulate drag during the coast phase following motor burnout. Plate deployment is actuated by a single servo mechanism coupled to an Archimedes spiral transmission, providing a predictable linear relationship between servo rotation and airbrake extension. A feedback-based control strategy uses onboard inertial and barometric measurements to estimate vehicle state and command airbrake deployment in real time. Key design considerations, including aerodynamic modeling, structural constraints, sensor integration, and fail-safe behavior are examined. Simulation results demonstrate precise apogee control for a subscale test vehicle, with the feed-forward PD controller tracking 900-1000m apogees with a maximum error of 2.5%. This indicates that the airbrake system is capable of greatly improving altitude targeting performance for suborbital experimental rockets.

I. Introduction

Achieving precise control and adhering to an ideal flight path is a fundamental challenge for varying missions and flight objectives. This is especially true in high-power experimental rocketry, particularly for missions with defined altitude limits such as those imposed by competition requirements. Accurate control of a rocket's ascent profile allows for repeatability, improves safety, and ensures collected data quality, and is therefore critical in environments where performance is evaluated for altitude accuracy rather than maximum achievable height

The work presented in this paper was motivated by the development of a suborbital rocket intended for the International Rocket Engineering Competition (IREC) in the 10,000-ft Commercial-Off-The-Shelf (COTS) motor category. Teams competing in this category share the goal of reaching the 10,000-ft target apogee as closely as possible while designing around commercially available solid rocket motors. Passive design approaches, even when supported by extensive simulations, often fail to reliably hit a consistent apogee due to unavoidable real-world uncertainties. Sources of apogee error include variability in motor thrust curves, atmospheric density fluctuations, wind-induced trajectory deviations, weathercocking, vehicle mass variation, launch rail alignment errors, many of which cannot be predicted with sufficient accuracy prior to flight. As a result, many modern solid-propellant rockets targeting tight altitude control employ active drag modulation techniques. By intentionally designing the vehicle to overshoot the target apogee, onboard sensing and feedback control techniques can reduce altitude error during flight.

This paper presents the design and analysis of an active airbrake system that modulates aerodynamic drag during the coast phase. An Archimedean spiral transmission driven by a single servo motor provides a predictable, near-linear mapping between servo angle and deployed airbrake area. This transmission strategy, coupled with a feedback-based control algorithm using onboard inertial and barometric sensing, minimizes mechanical and software complexity relative to more elaborate control architectures while still maintaining tight apogee control.

II. System Overview

The airbrake system is designed for integration into a 10,000-ft class suborbital competition rocket approximately 14 ft in length with a 6 in diameter airframe. The full-scale vehicle is powered by a commercial M-class solid rocket motor and follows a conventional flight profile. Notably, the airbrakes are only allowed control authority solely during the

*Undergraduate Student, Daniel Guggenheim School of Aerospace Engineering, AIAA Student Member (ID 1922033).
†Undergraduate Student, Daniel Guggenheim School of Aerospace Engineering, AIAA Student Member (ID 1744177).

coast phase between motor burnout and the detection of apogee. This restriction on deployment during the boost phase is deliberately placed to avoid excessive aerodynamic loads and structural stress on the airbrake plates. Furthermore, once apogee is detected, the system commands full retraction to eliminate the risk of interference with recovery system deployment.

The airbrake module consists of four aerodynamically symmetric plates arranged along the circumference of the airframe. Upon activation, the plates are designed to deploy horizontally into the freestream, increasing vehicle drag while avoiding net roll or pitch moments via design symmetry. All four plates are actuated simultaneously using a single high-torque servo motor through a mechanically linked transmission system. The Hiwonder HPS-3518SG high-speed coreless servo, rated at approximately 35 kg·cm torque, was chosen to drive the system based on conservative estimates of aerodynamic loading under maximum dynamic pressure conditions.

III. Mechanical Design

Each airbrake plate is approximately square in shape and has a surface area of around 4.25 square inches. The four plates are positioned at 90-degree intervals around the airframe and are rotationally offset from the fin plane to reduce any potential aerodynamic interference effects. Drag modulation is achieved by varying the percent area of the plates exposed to the freestream. In the fully retracted configuration, the vehicle drag coefficient is approximately equal to that of the baseline rocket configuration, $C_{D,r}$. As the plates deploy, the effective drag coefficient increases according to

$$C_D = C_{D,r} + k * C_{D,b}, \tag{1}$$

where $C_{D,b}$ represents the drag contribution of the airbrakes when fully extended and k represents the fraction of the brake area exposed to the flow.

In order to minimize adverse stability effects, the airbrake module is positioned such that it lies aft of the vehicle center of gravity and forward of the fin set. Both mechanical and software stops limit servo rotation to a commanded range of 30° to 150°, avoiding operation near hard servo limits.

A. Transmission Architecture and Design Rationale

A single-servo architecture was selected with the intent of minimizing mechanical complexity, mass, and potential failure points. Because the airbrake system is designed solely for apogee targeting rather than the more complex process of trajectory steering, closed-loop control of pitch or yaw was deemed unnecessary. As stated previously, the rocket was intentionally designed with a maximum uncontrolled apogee that exceeded the 10,000-ft target, allowing leeway for the controller to operate exclusively on vertical state estimation (altitude and vertical velocity) during the coast phase.

By deliberately designing to produce conservative static stability margins (with the intended rocket for this system having a stability margin of 10.5%), we allow for aerodynamic restoring forces to naturally suppress off-axis deviations. This reduces the need for thrust vectoring or aerodynamic vectoring corrections, which in turn enables the airbrake system to focus strictly on modulating axial drag as a method of controlling vertical apogee. This design philosophy helps significantly simplify both sensing requirements and control logic.

B. Spiral Cam Geometry and Kinematic Mapping

The transmission mechanism consists of a rotating actuator plate featuring guiding slots with the shapes of Archimedean spirals,

$$r = a + b\theta, \tag{2}$$

where r represents radial displacement and θ is the servo rotation angle. Linear bearings constrained within these slots convert rotational motion into linear extension of the airbrake plates, with the net effect being an approximately linear mapping between servo angle and brake extension. A servo then drives a central shaft coupled to this spiral actuator plate to govern deployment.

The key advantage of the Archimedean spiral profile (as illustrated by the earlier equation) is the approximately linear relationship between servo rotation and radial follower displacement that it enforces. This relationship, combined with the nearly square planform of the airbrake plates, allows for the linear extension to correspond closely to a linear increase in projected drag area. This near-linear relationship substantially simplifies aerodynamic modeling and controller implementation because brake area can be treated as proportional to commanded servo angle over the operational range.

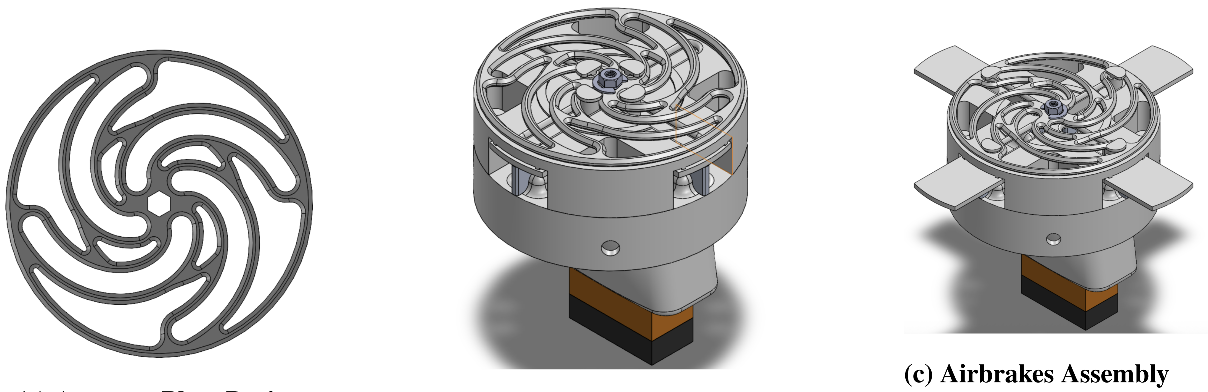

(a) Actuator Plate Design **(b) Airbrakes Assembly (Retracted Configuration)** **(c) Airbrakes Assembly (Deployed Configuration)**

Fig. 1 Airbrakes assembly depicting mechanical components and deployment configurations.

Figure 1a depicting the actuator plate also highlights the incorporation of mass reduction features wherever structurally permissible, minimizing rotational inertia without compromising stiffness or bearing support integrity.

C. Friction, Backlash, and Actuation Torque

Given that frictional force would be a major factor in sizing the servo, internal mechanical friction was strategically minimized through the use of linear bearings and lubrication at sliding interfaces. This ensured the dominant resistive load was limited to aerodynamic forces acting on the brake plates and minor contact interaction between the brake edges and airframe guides, both of which are inherent consequences of this design that are difficult to mitigate further.

Worst-case torque was evaluated under maximum dynamic pressure conditions, including initial deployment into high-speed airflow, full deployment at peak dynamic pressure, and retraction under high-speed flow. The calculated peak aerodynamic moment was multiplied by a safety factor of 2 to account for transient flow effects, manufacturing tolerances, and unmodeled aerodynamic coupling. The selected servo therefore provides sufficient torque margin to ensure reliable actuation under all anticipated flight conditions.

D. Structural and Material Considerations

Structural sizing of the airbrake plates accounted for aerodynamic bending loads, vibrational excitation during coast, and potential aerodynamic heating effects. Candidate materials include 6061-T6 aluminum or polycarbonate, which balance stiffness, mass, and manufacturability. For subscale validation flights, high-infill PLA printed components were deemed acceptable for preliminary testing. Fastening integrity was maintained using nylon-insert locknuts and threadlocker to resist vibration-induced loosening. Mechanical stops were integrated into the transmission to prevent overextension in the event of software or servo malfunction, providing a redundant physical safeguard against structural overstress.

IV. Electrical Design

The airbrake system involves three primary electrical subsystems: sensing, actuation and control, and data logging. The core hardware elements include a high-torque servo actuator, a barometric pressure sensor, an inertial measurement unit (IMU), and a microSD card module for onboard data logging. An Arduino-class microcontroller development board (Arduino Uno) was chosen to interface with these components and execute the flight control algorithm.

A. Power System Architecture

The previously mentioned Hiwonder HPS-3518SG 35 kg·cm servo motor requires an operating voltage between 5–8.4 V and can draw peak currents of approximately 2–3 A under load. To ensure adequate current delivery and prevent voltage sag during high-torque actuation, the servo was powered independently from the logic electronics using two 18650 lithium-ion cells (3.6–3.7 V nominal each) wired in series. The microcontroller and sensing electronics were powered separately using a 9 V battery connected to the Arduino Uno. The onboard voltage regulation circuitry provided stepped-down logic voltages for the IMU, barometer, and SD card module. This separation of actuation and logic power systems reduced susceptibility to electrical noise and brownout conditions caused by transient servo loads.

B. Sensors and State Estimation Hardware

State estimation relied on a combination of barometric altitude sensing and inertial acceleration measurements. A BMP280 barometric pressure sensor was used to provide altitude measurements relative to a calibrated ground reference, with adequately sized static pressure ports that ensured accurate pressure sampling during flight. Inertial measurements were obtained using an Adafruit LSM6DS3TR-C six-degree-of-freedom IMU, providing three-axis accelerometer and gyroscope data. Acceleration measurements were used by the state machine for launch detection, motor burnout detection, and vertical velocity / apogee detection.

Sensor sampling rates were selected to ensure adequate temporal resolution during boost and coast phases while remaining within the processing limits of the microcontroller. Noise characteristics of both sensors were considered when designing filtering and detection logic.

C. Electronics Sled Design

All avionics components were mounted on a dedicated electronics sled designed in SolidWorks and 3D printed at 10% infill to minimize mass. The sled incorporates recessed mounting features tailored to each component's dimensions and threaded inserts for secure fastening. The sled was installed within a coupler section immediately above the airbrake module to minimize wiring length, reduce signal routing complexity, and centralize system integration. Appropriately sized static pressure taps were drilled through the coupler to provide accurate barometric measurements during flight.

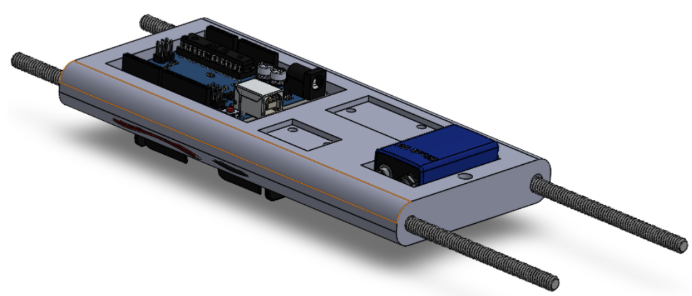

Fig. 2 SolidWorks model for electronics sled

V. Software Design

The software components of the airbrake architecture consists of three primary programs: (1) a reduced flight-phase state machine governing when airbrake operations are permitted, (2) a hybrid feedforward–feedback control algorithm for apogee regulation during coast, and (3) a hardware-in-the-loop (HIL) simulation framework used for controller tuning and validation. Because physical test-based tuning of apogee control is impractical and cost-prohibitive, the HIL framework played a key role in gain selection and controller verification.

A. Flight Phase Detection Logic

The supervisory logic was implemented as a finite state machine consisting of an initialization phase followed by four primary states: waitUntilLaunch (idle / armed state), waitUntilMotorBurnout (boost phase), airbrakeActive (coast phase), and recovery (apogee and post-apogee phase). Additional states beyond apogee were deemed unnecessary, as the airbrakes are commanded to fully retract once apogee is detected. The basic sensor-based detection logic was defined as follows:

- Launch detection is triggered by IMU acceleration exceeding a predefined threshold.
- Motor burnout detection occurs when measured acceleration returns to approximately 1 g.
- Apogee detection is declared when estimated vertical velocity crosses zero.

To improve robustness, a timer-based guard condition for motor burnout was implemented based on manufacturer-specified burn duration data, with a small delay margin. Similarly, airbrake deployment was also limited to a predefined time window, after which the system would automatically command retraction in the event that apogee detection failed due to barometric error. Furthermore, automatic retraction is hardcoded as a safety against the event of any anomalous altitude readings. Together, these safeguards provide redundancy in state determination and mitigate the effects of potential sensor faults at a level appropriate for a mechanically simplified experimental system.

B. State Estimation

Altitude is computed from barometric pressure relative to a calibrated ground reference and subsequently smoothed via low-pass filtering to reduce high-frequency noise in both barometric and inertial measurements. Vertical velocity is estimated through numerical differentiation of the filtered altitude signal.

Apogee prediction uses a simplified ballistic model derived from energy methods:

$$h_{\text{predicted}} = h + \frac{v^2}{2g}(1 - k), \tag{3}$$

where k is a drag correction factor that approximates the effect of baseline body drag with 0% brake extension. This bases control logic on the altitude the rocket would reach if no brake drag was applied from the current timestep onward.

C. Control Law

As the first few seconds after burnout prove crucial to accurate apogee control, especially with a system that deliberately reaches an apogee higher than the target when uncontrolled, a hybrid feedforward–feedback architecture was selected to ensure rapid response immediately following burnout. The feedforward component estimates the predicted apogee from the current velocity and determines an initial brake extension using a precomputed apogee-to-angle lookup table. This feedforward term initially dominates to quickly reduce predicted apogee, and the coupled PD controller subsequently trims the relatively small residual errors that arise during the coast phase due to atmospheric variability, modeling inaccuracies, and sensor noise. Because the active control window is short and non-steady-state, the integral term was deliberately excluded; integral accumulation could produce rapid windup without sufficient time for unwinding. Thus, avoiding integral action reduces complexity and improves predictability.

1. Error Definition

At each control timestep, the predicted apogee altitude is estimated using Equation 3. The control error is defined as:

$$e = A_{\text{predicted}} - A_{\text{target}}, \tag{4}$$

where a positive error corresponds to an expected apogee overshoot (commanding increased drag), and a negative error indicates an undershoot (commanding retraction).

2. Feedback Formulation

The feedback controller is implemented as a proportional–derivative (PD) law:

$$\Delta\theta = K_p e - K_d v, \tag{5}$$

where θ is the servo angle, v is the current vertical velocity, and K_p and K_d are the proportional and derivative gains, respectively. Unlike classical dimensionless control gains, the gains in this formulation retain physical units: K_p has units of degrees per meter, and K_d has units of degrees per (m/s). The advantage of this form will become apparent in the discussion of HIL methods.

Servo commands are bounded to 30°–150° to avoid mechanical end stops. Saturation is implemented directly without integral accumulation, eliminating the need for anti-windup logic. Although explicit rate limiting was not implemented, it was deemed unnecessary. Immediately after burnout, a single feedforward with built in delay command governs deployment, and subsequent PD trim adjustments are sufficiently small that actuator speeds have negligible impact on performance. Furthermore, the servo's inherent angular velocity limit provides a natural bound on command rate, eliminating the need for additional software constraints.

3. Gain Selection via Hardware-in-the-Loop Simulation

Traditional tuning methods such as Ziegler–Nichols or ultimate gain testing are impractical for apogee control in high-power rocketry, with each tuning iteration requiring a full flight test. Given the cost and limited opportunities associated with test flights, an alternative gain selection strategy was therefore sought. The key insight here became a reevaluation of the physical form of the controller. As discussed above, the gains in the $K_p e - K_d v$ formulation retained physical units, and these units provide immediate insight into bounds on feasible gain magnitudes. During the coast phase, typical signal magnitudes are on the order of $e \sim 10$–100 m and $v \sim 100$–200 m/s. Excessively large gain values would therefore command servo deflections approaching saturation. Consequently, the practical gain range is bounded by the ratio of available actuator authority to expected signal magnitude. This observation significantly narrows the feasible parameter space.

With the gain space constrained to physically plausible values, a hardware-in-the-loop (HIL) based sweep over the sample space could be employed to systematically evaluate controller performance. The HIL framework propagates vertical vehicle dynamics forward in discrete timesteps. At each timestep:

1) The controller computes a servo command.
2) Aerodynamic drag is updated as a function of airbrake extension.
3) The vehicle state (altitude and velocity) is propagated forward.

This loop repeats until apogee detection.

Gain combinations were swept over the constrained ranges

$$K_p \in [0.2, 0.8], \qquad K_d \in [0, 0.08].$$

For each gain pair, the simulated flight was propagated to apogee and the resulting altitude error recorded. The resulting error surface was visualized as a two-dimensional heat map of apogee error versus (K_p, K_d). The boundary regions above 10 meters of error corresponded to control saturation and ineffectiveness; regions exhibiting low mean error and robustness to small perturbations were identified and selected for implementation. This approach enabled systematic controller tuning while avoiding the cost and impracticality of iterative flight-based testing.

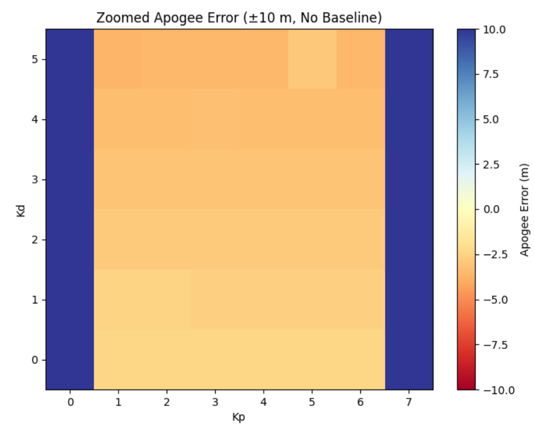

Fig. 3 Heatmap showing effectiveness of gain pairs

D. Safety and Fail-Safe Behavior

Safety mechanisms were implemented at both hardware and software levels to prevent unintended interference with flight-critical systems. The airbrakes default to a fully retracted configuration under all fault conditions, including watchdog timeouts, brownouts, invalid sensor readings, or state transitions outside the permitted coast phase. Deployment is inhibited outside this window, and any anomalous condition immediately commands retraction. Mechanical stops provide an additional physical safeguard against unintended over-extension.

VI. Simulation and Performance Analysis

A. Vehicle Configuration and System Description

The airbrake system was scaled to fit in a Level 2 (L2) high-powered rocket for testing. This vehicle category was selected based on material availability and cost considerations. Although the test vehicle requires less drag production from the airbrakes than the intended competition vehicle due to its lower overall mass, this configuration is expected to yield representative aerodynamic data which can be used to validate the mechanical design and the software of the airbrakes system.

An OpenRocket model of the test vehicle was developed to provide an initial estimate of the rocket's mass distribution and inertial properties (see Figure 4). The airbrake system is located within the aft-most 20m coupler section, positioned above the motor casing.

The vehicle components were individually massed, resulting in a total loaded mass of 6.1kg. The center of gravity (CG) was estimated at 1.71m from the nose tip on the pad and 1.55m at burnout. The total longitudinal and rotational inertias, 2.17kg·m^3 and 0.01kg·m^3 respectively, were also estimated with OpenRocket, summing the contribution of all components at the vehicle's center of gravity, considering each component's shape and mass [1]. These parameters are used for the following aerodynamic and flight-dynamics analyses.

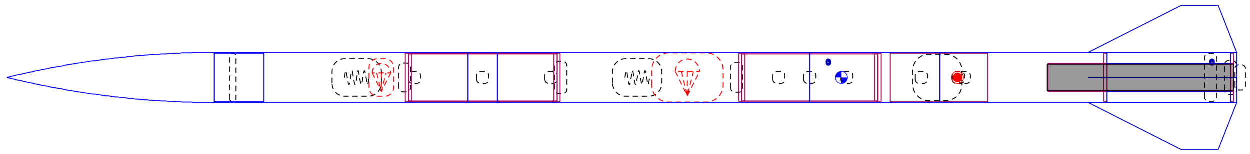

Fig. 4 OpenRocket model of the L2 validation vehicle.

B. Aerodynamic Modeling

1. Static Stability Analysis

Barrowman's slender-body method is applied under its standard assumptions of small angle of attack, steady and irrotational subsonic flow, rigid-body motion, and sharp-tipped nose [2]. These conditions are approximately satisfied for the test vehicle during majority of the ascent, as the rocket maintains relatively small angles of attack and remains fully subsonic ($M_{\max} \approx 0.66$). Under these assumptions, the Barrowman method was used to compute the normal force coefficient slope C_{N_α} and center-of-pressure location for the test vehicle. The rocket was decomposed into nose, body, fins, and airbrake plates, each represented by an equivalent slender-body or flat-plate element. For each component i, the incremental normal force slope $C_{N_{\alpha,i}}$ and axial location x_i were evaluated and combined to obtain the total C_{N_α} and aggregate CP location

$$C_{N_\alpha} = \sum_i C_{N_{\alpha,i}} \quad \text{and} \quad x_{CP} = \frac{\sum_i C_{N_{\alpha,i}} x_i}{\sum_i C_{N_{\alpha,i}}}. \tag{6}$$

Each airbrake plate was modeled as a small flat lifting surface with projected planform area S_{AB} and axial moment arm measured from the nose tip. Under the small angle of attack assumption, the normal force coefficient slope is

$$C_{N_{\alpha,\text{plate}}} = c_{n\alpha} \frac{S_{AB}}{S_{\text{ref}}}, \tag{7}$$

where $c_{n\alpha}$ is usually 2π per radian for a thin flat plate, and S_{ref} is the rocket reference area taken from the largest diameter. From thin airfoil theory, the center of pressure of a flat plate is at its geometric center since the pressure distribution is approximately symmetrical about the mid-chord point [3]. The airbrake normal force and CP terms were combined with the nose cone, body tube, and main fin contributions per Equation (6) to yield the overall C_{N_α} and x_{CP} for both stowed ($C_{N_{\alpha,AB}} = 0$) and fully deployed airbrake configurations, as presented in Table 1.

Table 1 Barrowman Normal Force Coefficient Slopes and Center of Pressure Locations

Component	C_{N_α}	x_{CP} (m from nose tip)
Nose Cone	2.00	0.198
Main Fins	8.76	2.348
Airbrakes (Deployed)	0.19	1.960
Total — Stowed	10.76	1.948
Total — Deployed	10.95	1.949

The airbrakes have a very small effect on the CP location since the normal force coefficient derivative of 0.190/rad is relatively small (only 2.1% of the total) due to the small planform area. Nonetheless, to minimize possible destabilizing effects, the airbrakes were placed behind the center of gravity (see Figure 4), hence why CP increases with airbrake deployment.

The stability margin can be calculated as

$$SM = \frac{x_{CP} - x_{CG}}{L} \cdot 100\%, \tag{8}$$

where the stability margin is expressed in percentage of body length. At the time of writing, IREC regulations require a minimum stability margin of 7% and maximum of 18% on the pad. The stability margin is estimated to be 15.83% at burnout, well within requirement bounds.

2. Airbrake Drag Coefficient Modeling

For bluff-body airbrakes, drag is generated primarily by the pressure difference across the plate normal to the flow. The drag force is the streamwise component of the pressure force acting over the plate's surface ($D = N \sin\theta$). The projected area scales according to the linear deployment law $r = a + b\theta$:

$$S_\perp(\theta) = S_{\max}\frac{r(\theta) - a}{r_{\max} - a} = S_{\max}\frac{b\theta}{b\theta_{max}}\sin\theta. \tag{9}$$

The maximum attainable normal force coefficient for a bluff-body plate is 1.28, giving

$$C_{\mathrm{D,AB}}(\theta) = \frac{D(\theta)}{q_\infty S_{\max}} = \frac{C_{n_{\max}} q_\infty S_\perp(\theta)\sin\theta}{q_\infty S_{\max}} = 1.28\frac{\theta}{\theta_{\max}}\sin^2\theta. \tag{10}$$

3. RASAero Aerodynamic Simulations

The L2 rocket was modeled in RASAero, maintaining the configuration from the OpenRocket model. The airbrakes were approximated as rectangular fins of span 0.95in, chord 0.1in and thickness 1.0in.

The normal force coefficient slope was evaluated at stowed and deployed configurations to isolate the airbrake contribution. C_{N_α} in the stowed configuration was 14.53/rad, while for fully-deployed configuration it was 14.77/rad. This gives an airbrake contribution of 0.24/rad for subsonic flow, slightly greater than the thin airfoil theory estimate (0.19/rad), but small enough that the airbrakes will not destabilize the vehicle.

The drag coefficient vs Mach number was extracted for the stowed vehicle, and deployment increments of 0.25. To isolate the airbrake drag contribution, the stowed C_d curve was subtracted from each configuration. The resulting drag as a function of deployment level and Mach number was plotted in Figure 5.

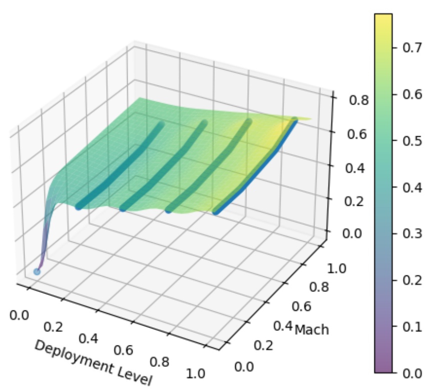

Fig. 5 C_D **from airbrakes as a function of deployment and Mach number**

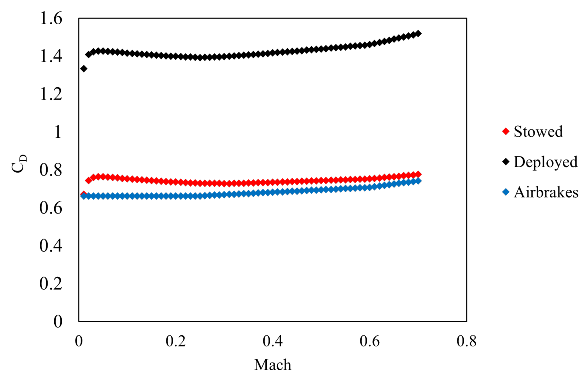

Fig. 6 Drag coefficient comparison between stowed and deployed configuration

The airbrake drag coefficient when fully deployed ranges from 0.7 to 0.8. Although this differs significantly from the bluff-body approximation of 1.28, it is consistent with the results obtained by Sprague et al. [4], and sufficient for a noticeable effect on the vehicle's apogee.

C. Trajectory Simulations

1. Simulation Setup and Modeling in RocketPy

The trajectory was studied using RocketPy, an open-source Python-based 6DoF flight dynamics tool. RocketPy performs trajectory integration using a built in Runge-Kutta-Fehlberg (RK45) solver with adaptive time-stepping

The simulation used the Global Ensemble Forecast System (GEFS) to extract temperature, pressure and wind profiles for specific locations at 12h intervals, providing realistic launch-day atmospheric conditions. The launch angle was set to 85° from the ground to account for expected deviations during launch.

The aerodynamic coefficients for the vehicle were extracted from RASAero, and a drag look-up table (LUT) was implemented for the airbrakes, listing the drag coefficient at different deployment levels and Mach numbers.

2. Airbrake Controller Function Implementation

The controller receives the rocket state $\mathbf{u}$ at each timestep from the 6-DOF integrator,

$$\mathbf{u} = \begin{pmatrix} x & y & z & v_x & v_y & v_z & e_0 & e_1 & e_2 & e_3 & \omega_1 & \omega_2 & \omega_3 \end{pmatrix}. \tag{11}$$

which contains the position (x, y, z) and velocity (v_x, v_y, v_z) of the vehicle in the NED frame. The controller operates as a sequential state machine through three phases: powered ascent, hold and active trim. The airbrakes do not deploy during motor burn. The controller monitors acceleration by extracting the vertical velocity components from the state vectors for two consecutive time steps and computing the finite difference

$$a_k = \frac{v_{z,k} - v_{z,k-1}}{\Delta t}. \tag{12}$$

When the vehicle has exceeded the minimum velocity threshold and the calculated acceleration satisfies $a_k < a_{\text{thresh}} = -2\text{m/s}^2$, motor burnout is declared. At this state, the net axial force has become negative, hence thrust has dropped to zero. When burnout is detected, a feed-forward servo command is initialized. The controller queries a pre-computed lookup table, which maps target apogee to the required brake deployment angle for each altitude. The LUT was populated by performing an empirical sweep an empirical of constant-deployment trajectory simulations. Each entry records the apogee altitude achieved at a given servo angle under expected launch day conditions. For a given target apogee A_{target}, the feed-forward command is obtained by linearly interpolating between the two nearest LUT entries

$$\theta_{FF} = \theta_i + \frac{A_{\text{target}} - A_i}{A_{i+1} - A_i} \left(\theta_{i+1} - \theta_i\right). \tag{13}$$

The deployment level passed to the RocketPy actuator model remains constant for the first 200ms ($\theta_{\text{cmd}} = \theta_{\text{FF}}$, giving the state variables time to settle before the feedback loop is closed. After the hold period, the controller enters the active trim phase. Each time step, the apogee at the current configuration is estimated through a simple ballistic model shown in Equation (3). Although this estimator applies an energy conservation model that neglects drag, this model yields a predicted apogee A that is always greater than the actual value. This introduces a positive bias into the system that causes the airbrakes to stay deployed during the coast phase, avoiding their possible retraction due to noise in the error signal e (see Equation (4). A PD correction is applied to this error term in addition to the feed-forward command, giving the servo command passed to the simulation at each time step

$$\theta_{\text{cmd}} = \underbrace{\theta_{FF}}_{\text{feed-forward}} + \underbrace{K_p \cdot e - K_d \cdot v_z}_{\text{PD trim}}, \tag{14}$$

with gains $K_p = 0.4$ and $K_d = 0.03$. This also causes a natural retraction of the airbrakes as $v_z \to 0$, since the derivative term drives θ_{cmd} back toward θ_{FF}, preventing excessive deployment when the airbrakes produce little effect on the apogee due to the low dynamic pressure. The servo command is constrained to the physical servo range $\theta_{\text{cmd}} \in [60°, 120°]$, preventing the airbrake from commanding a physically impossible deployment. This is then converted to a normalized deployment level $d \in [0, 1]$ via

$$d = \frac{\theta_{\text{cmd}} - \theta_{\text{min}}}{\theta_{\text{max}} - \theta_{\text{min}}}. \tag{15}$$

This deployment level is passed to the RocketPy airbrake actuator at each time step, updating the aerodynamic drag contribution of the airbrakes used in the integration for the next state throughout the entire flight simulation.

3. Simulation Results

The following figures display the deployment set by the controller function at each timestep, as well as the flight profile for different target altitudes.

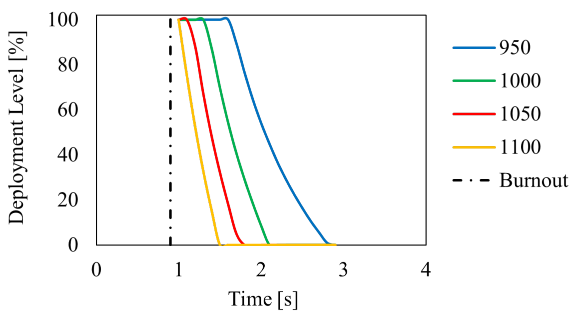

Fig. 7 Deployment vs time for varying target altitudes

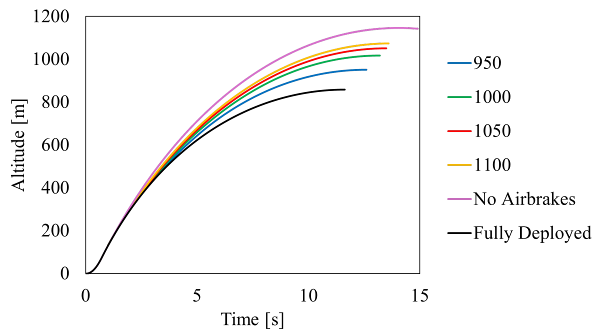

Fig. 8 Altitude vs time for varying target altitudes

Figure 7 shows the progression of the state machine. The airbrakes are fully stowed during the burn phase. After burnout, the airbrakes fully extend, remaining on hold for 200ms before progressively trimming. This trimming process takes longer for lower target apogees, since more drag production is needed.

Figure 8 contains the flight profiles of the vehicle for different target apogees set in the controller function, as well as the profile for the cases in which the airbrakes do not deploy (A_{max}) and for which the airbrakes stay fully opened from burnout to apogee (A_{min}). The achieved apogee values for all cases are compiled in Table 2.

Table 2 Achieved apogees for varying target apogees

Target Apogee [m]	Achieved Apogee [m]	Absolute Error [m]	Relative Error [%]
900	886	-14	-1.6
950	951	+1	+0.1
1000	1017	+17	+1.7
1050	1057	+7	+0.7
1100	1073	-27	-2.5
Fully deployed (100%)	859	–	–
Fully stowed (0%)	1147	–	–

The controller demonstrates excellent tracking performance across the 900-1100 m operating range, achieving a maximum error of 2.5% between target and simulated apogees. Notably, the system is sufficiently sensitive when operating near the achievable apogee bounds, allowing the user to confidently target altitudes close to these boundaries. The empirical energy dissipation term k, set to 0.4 in the simulations, prevents the airbrake system from being deployed for an excessive amount of time. If k where set to 0, the controller would predict apogees way lower than the attainable altitudes at any point in time, therefore favoring deployment and causing the vehicle to undershoot the target.

D. Assumptions and Model Limitations

Further aerodynamic analysis is required for a full-scale IREC vehicle. Since these typically operate in the transonic and supersonic regimes, aerodynamic analyses reliant on semi-empirical methods may not hold due to shock formation, wave drag and flow separation causing significant alterations to axial and normal forces. The deployed airbrake geometry introduces flow effects that may not be captured by these methods, leading to under prediction on drag and significant changes in stability. At higher angles of attack, nonlinear lift and drag effects as well as flow separation may arise, causing significant variations to the static margin and drag characteristics of the vehicle

The empirical approach for the correction of the energy conservation equation used to predict apogee by the controller may be sufficient for the simulated conditions. However, this embeds inaccuracies into the control law that may not hold under different sets of conditions. The correction factor k used may thus only be valid for this particular L2 vehicle and for the simulated conditions

Collectively, these limitations suggest that while the present analysis is adequate for preliminary validation of the airbrake concept, higher-fidelity aerodynamic modeling and experimental validation is necessary to ensure robustness and scalability of the system.

VII. Discussion

Both simulation and hardware-in-the-loop results showcase that active drag modulation significantly reduces apogee error compared to an uncontrolled ascent. After proper tuning of the controller, apogee error was reduced to within 3 m under nominal conditions, indicating effective mitigation of modeling uncertainty and environmental variability.

The system exhibited low sensitivity to sensor noise due to the use of first-order low-pass filtering and the limited control authority exercised after the initial deployment phase. Observed variations in estimated velocity resulted in only minor servo corrections, indicating inherent robustness of the control formulation. While more advanced filtering techniques such as Kalman filtering could further improve state estimation accuracy through sensor fusion, they were not implemented due to microcontroller RAM limitations and increased development complexity.

Servo speed limitations were most influential immediately following motor burnout, when rapid drag deployment has the greatest impact on apogee correction. The feedforward-dominant control window mitigated this constraint, with subsequent PD trim adjustments being small enough that actuator rate limits had negligible influence on performance.

An initial subscale flight test targeting an apogee of ~3750 ft was conducted to validate system functionality. Post-flight data analysis revealed intermittent velocity estimation errors caused by sensor sampling rate mismatches. After correcting the datasets, follow-up simulations confirmed the intended control logic functioned as designed. Subsequent revisions addressed this issue through synchronized sensor sampling and additional plausibility filtering.

From a scalability perspective, the airbrake architecture presents minimal barriers to adaptation for higher-performance vehicles. Scaling would primarily require recalculation of aerodynamic loads, appropriate servo resizing based on revised torque requirements, and material selection adjustments for increased dynamic pressure environments. The overall mechanical transmission concept and control strategy remain directly transferable.

Future improvements include development of a custom printed circuit board to improve electrical robustness and expand available memory, enabling implementation of more advanced state estimation techniques such as Kalman filtering and more sophisticated state-machine logic. Mechanically, incorporation of a passive spring-based retraction mechanism would provide inherent fail-safe behavior, ensuring automatic brake retraction in the event of power loss.

VIII. Conclusion

In conclusion, this paper presented the design and analysis of a simplified active airbrake system for controlling the apogee of a 10,000-ft class suborbital rocket. The integration of mechanical, electrical, and software design proved an effective strategy in reducing apogee error and improving flight repeatability. The system is well-suited for both experimental and competition rockets, as well as other applications where precise altitude targeting may be required.

Acknowledgments

AI was employed to paraphrase and reword key concepts, but all conceptual information was developed by the authors. All technical data and provided figures were also developed by the authors. The airbrakes system and relevant simulations discussed in this paper were designed with Georgia Tech's Ramblin' Competition Rocketry team as the primary application. However, the specific content described in this paper was developed by Yuvasurya R. Vangala and Alonso Arregui Martinez.

References

[1] Niskanen, S., "Development of an Open Source model rocket simulation software," Ph.D. thesis, Helsinki University of Technology, Espoo, May 2009.

[2] Barrowman, S., "The practical calculation of the aerodynamic characteristics of slender finned vehicles," Ph.D. thesis, The Catholic University of America, Washington, D.C., Mar. 1967.

[3] Hoerner, S. F., *Fluid-Dynamic Drag: Practical Information on Aerodynamic Drag and Hydrodynamic Resistance*, Published by Author, Brick Town, NJ, 1965.

[4] Sprague, T., Sanipara, N., and Belew, A., *Design and Analysis of a High-Powered Rocket Airbrake System*, 2024. https://doi.org/10.2514/6.2024-85628.